Journal of Materials Chemistry C

Check for updates

Efficient third harmonic generation from FAPbBr₃ perovskite nanocrystals†

Andrea Rubino,‡[a] Tahiyat Huq,‡[b] Jakub Dranczewski, [b] Gabriel Lozano, [a] Mauricio E. Calvo, [a] Stefano Vezzoli,[b] Hernán Míguez *[a] and Riccardo Sapienza*[b]

The development of versatile nanostructured materials with enhanced nonlinear optical properties is relevant for integrated and energy efficient photonics. In this work, we report third harmonic generation from organic lead halide perovskite nanocrystals, and more specifically from formamidinium lead bromide nanocrystals, ncFAPbBr₃, dispersed in an optically transparent silica film. Efficient third order conversion is attained for excitation in a wide spectral range in the near infrared (1425 nm to 1650 nm). The maximum absolute value of the modulus of the third order nonlinear susceptibility of ncFAPbBr₃, $\chi^{(3)NC}$, is derived from modelling both the linear and nonlinear behaviour of the film and is found to be $\chi^{(3)NC} = 1.46 \times 10^{-19}$ m² V⁻² (or 1.04×10^{-11} esu) at 1560 nm excitation wavelength, which is of the same order as the highest previously reported for purely inorganic lead halide perovskite nanocrystals (3.78×10^{-11} esu for ncCsPbBr₃). Comparison with the experimentally determined optical constants demonstrates that maximum nonlinear conversion is attained at the excitonic resonance of the perovskite nanocrystals where the electron density of states is largest. The ease of synthesis, the robustness and the stability provided by the matrix make this material platform attractive for integrated nonlinear devices.

Introduction

Halide perovskites offer an interesting platform as nonlinear optical materials[1] due to their favourable photophysical properties, such as strong absorption above bandgap,[2] high dielectric constant[3] and the presence of strong excitonic resonances. In particular, high bandgap perovskites[4,5] and systems confined with a high binding energy[6] and large oscillator strength,[7] should give rise to an excellent nonlinear performance. The centrosymmetric crystal structure of halide perovskites allows for third-order nonlinear effects, such as third harmonic generation (THG), light induced modulation and saturable absorption in single crystals of bulk material,[8] polycrystalline thin films[9] and 2D layered perovskites.[10] Furthermore, one of the advantages of organic–inorganic lead (Pb) halide perovskites is that versatile chemical composition APbX₃ with the easily changeable cation A (methylammonium, formamidinium, cesium) and anion X (chlorine, bromine, iodine) allows for improved stability,[11] control over the photophysical properties in the visible spectrum,[12] and a reversible bandgap tunability,[13] features that are relevant for the development of light emitting devices.[14] In this context, formamidinium-based perovskites have already demonstrated greater stability than their paradigmatic methylammonium-based counterparts, which makes them particularly interesting for optoelectronic applications based on their photoemission properties.[15]

Alternatively, reducing the crystal size, if comparable to the characteristic exciton Bohr radius of the semiconductor, provides another way of tuning the spectral position of the third harmonic through the electronic bandgap shift resulting from quantum confinement effects. This approach makes unnecessary changing the chemical composition, thus avoiding problems related to phase segregation or structural instability.[13] In this context, efficient second and third order optical nonlinearities have been observed for all inorganic CsPbX₃ nanocrystals (ncCsPbX₃), where X = Cl, Br or I,[16] with maximum nonlinear conversion efficiencies and susceptibilities being reported for CsPbBr₃ nanocrystals.[17]

In this work, we report evidence of THG from ligand free organic lead halide perovskite nanocrystals. We employ formamidinium lead bromide (CH(NH₂)₂PbBr₃ or FAPbBr₃) perovskite nanocrystals with diameters below 10 nm embedded in a transparent porous thin film matrix made of SiO₂ particles. By varying the NIR excitation wavelength, efficient third order

[a] Institute of Materials Science of Seville, Consejo Superior de Investigaciones Científicas (CSIC)-Universidad de Sevilla (US), Américo Vespucio 49, 41092, Seville, Spain. E-mail: h.miguez@csic.es

[b] The Blackett Laboratory, Department of Physics, Imperial College London, London SW7 2BW, UK. E-mail: r.sapienza@imperial.ac.uk

† Electronic supplementary information (ESI) available: Details on the extraction of the third-order nonlinear susceptibility of FAPbBr₃ nanocrystals. See DOI: 10.1039/d0tc04790b

‡ These two authors contributed equally to this work.

15990 | *J. Mater. Chem. C*, 2020, **8**, 15990–15995

This journal is © The Royal Society of Chemistry 2020

emission is observed from ncFAPbBr$_3$ within the 475–550 nm wavelength range. We find that the highest value of the third order nonlinear susceptibility, $\chi^{(3)NC} = (1.46 \pm 0.19) \times 10^{-19}$ m^2 V^{-2} (*i.e.*, 1.04×10^{-11} esu), is similar to the best one reported so far for purely inorganic colloidal perovskite nanocrystals (3.78×10^{-11} esu for ncCsPbBr$_3$) (measured with *z*-scan),[1,17] whose processing is much more involved due to the presence of organic ligands. Interestingly, this occurs when excitation takes place at $\lambda = 1560$ nm and hence when the third order emission occurs at $\lambda/3 = 520$ nm, *i.e.*, when it matches the excitonic resonance. The third order nonlinear conversion efficiency, measured as the ratio between the power of the third harmonic and that of the pump laser, is 4.27×10^{-6} for a film of 1300 nm embedding ncFAPbBr$_3$ at 6.5 vol%. From a practical perspective, the system we present also offers the versatility and ease of fabrication necessary to make these materials attractive for technological applications or for integration into more complex architectures.

Results and discussion

Fabrication process

The fabrication process of perovskite nanocrystals consists of a template synthesis method using a porous matrix, as reported in a previous work.[18] The porous matrix structure is formed by a 1300 nm-thick highly uniform layer made of silicon dioxide (SiO$_2$) nanoparticles of 30 nm diameter deposited by dip coating (Fig. 1a) onto a glass substrate. This gives rise to an optically transparent porous film of 50% porosity that has been thoroughly analysed elsewhere.[18] Subsequently, a solution containing the FAPbBr$_3$ perovskite precursors is infiltrated into the matrix by spin-coating. A final thermal treatment at 100 °C promotes the rapid crystallisation of the perovskite within the pores. By controlling the concentration of the precursors solution that is infiltrated into the void space of the porous matrix and the final rotation speed, we assure that the formation of perovskite nanocrystals occurs exclusively inside the pores, avoiding the presence of macro-crystals on the surface. In what follows, we will refer to this composite as ncFAPbBr$_3$@SiO$_2$. The SiO$_2$ matrix has a multilayer structure which is visible *via* a cross-section in transmission electron microscopy, shown in Fig. 1b. As presented in Fig. 1c, the presence of perovskite nanocrystals is disclosed as brighter regions in the high-angle annular dark-field (HAADF) image. Perovskite nanocrystals inclusion in the matrix is also corroborated by the EDX lead mapping of the same section. The high-resolution micrograph presented in Fig. 1f illustrates that FAPbBr$_3$ nanocrystals present an average diameter of 9 nm. For the sake of comparison, we synthesized a FAPbBr$_3$ film using the same precursor solution directly spin-coated on a bare glass substrate.

The X-ray diffraction performed at a grazing angle on the ncFAPbBr$_3$@SiO$_2$ and bulk FAPbBr$_3$ films demonstrated that both samples have the same cuboid crystalline structure (Fig. 1g). Our synthetic strategy avoids the addition of organic ligands, characteristic of colloidal semiconductor nanocrystals,[19] and hence facilitates the analysis of the nonlinear properties of the ensemble. Simultaneously, self-aggregation is prevented, as
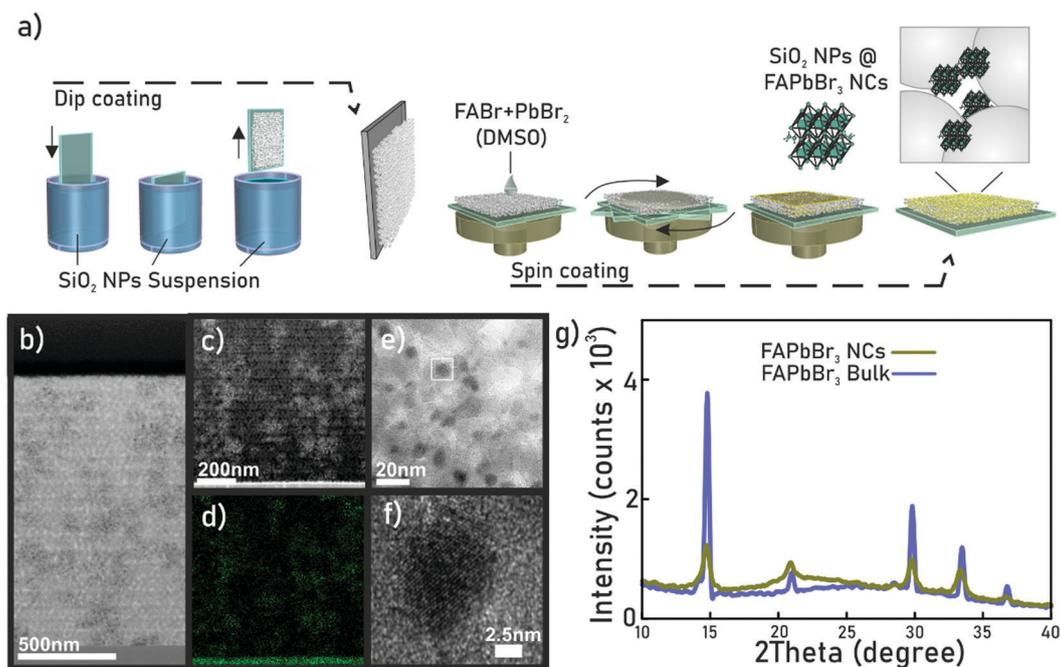

Fig. 1 Fabrication process. (a) Scheme of the ncFAPbBr$_3$@SiO$_2$ film fabrication process. (b) low magnification TEM cross section of a ncFAPbBr$_3$@SiO$_2$ film. (c) HAADF-STEM image of a cross section and (d) the corresponding Pb mapping using EDX. (e) HRTEM micrograph of a ncFAPbBr$_3$@SiO$_2$ film, in which nanocrystals can be seen. (f) A closer look to a single FAPbBr$_3$ nanocrystal. (g) XRD patterns of ncFAPbBr$_3$@SiO$_2$ (green line) and bulk (blue line) films.

the matrix also favours the dispersion of the nanocrystals.[18,20,21] Quantitative analysis of the elemental lead present in the film by Inductively Coupled Plasma Atomic Emission Spectroscopy (ICP-AES) reveals a 6.5 ± 0.1 vol% of $FAPbBr_3$ nanocrystals in the film, which implies that silica and air occupy 50% and 43.5% of the composite volume respectively.

Linear optics characterisation

$ncFAPbBr_3@SiO_2$ films show exciton quantum confinement effects, as evidenced in Fig. 2a, where a 45 meV blue-shift of the photoluminescence peak, with respect to that of the bulk perovskite, can be clearly seen. This results from the exciton wave function confinement inside the $FAPbBr_3$ nanocrystals. The emission spectral width also shows the absence of significant inhomogeneous broadening, hence supporting the presence of a narrow nanocrystal size distribution within the matrix. In parallel, Fig. 2b shows the absorptance of a $ncFAPbBr_3@SiO_2$ film (green line) and of a bulk, 300 nm thick, $FAPbBr_3$ film (blue line), estimated by measuring total reflection and total transmission with an integrating sphere (DRA-2500, Agilent) attached to a UV-Vis-NIR spectrophotometer (Cary 5000, Agilent). Please note that, consistently, a blue-shift of the absorption band edge is observed.

The refractive index, n, and extinction coefficient, κ, of the $ncFAPbBr_3@SiO_2$ film are obtained from the fittings of the measured optical reflectance and transmittance at different incidence angles (UMA, Agilent, Cary 7000),[22] and are displayed in Fig. 2c. Both n and κ increase sharply for energies above the bandgap, while for lower energies κ is imposed to be zero and n is approximately 1.315, which is consistent with the expected filling fractions of silica, air and semiconductor in the composite. Knowing the refractive index of the medium, as well as the

fill factor of each component, we can estimate the optical constants of the embedded $FAPbBr_3$ nanocrystals, obtained using the Forouhi–Bloomer model,[23] which will be later required to estimate its nonlinear coefficients.

Third-harmonic generation measurements

THG is the emission of a wave of frequency 3ω after excitation by an incident field of frequency ω (the pump), and it is mediated by the induced nonlinear polarisability, whose strength is quantified by the third order nonlinear susceptibility, $\chi^{(3)}$. In our case, an excitation laser source (Yb:KGW PHAROS, Light Conversion) with 200 fs pulses and 100 KHz repetition rate is pumping an optical parametric amplifier (ORPHEUS, Light Conversion), producing pulses with energy of 0.5–1 μJ, tunable between 1340 nm to 1740 nm. The THG from the $ncFAPbBr_3@SiO_2$ film is excited at normal incidence by focusing the pump laser down to a ∼68 micrometer (FWHM) spot. The THG signal in the transmission direction is coupled into a fiber spectrometer (Flame, Ocean Optics) or into a power-meter for measurements of absolute efficiency. A detailed sketch of the setup is presented as ESI.† The laser power, P_1^{laser}, is maintained at 15 mW for all pump wavelengths throughout the measurements, corresponding to an intensity of ∼7 GW cm^{-2}, well below the sample damage threshold (P_1^{laser} = 117 mW, corresponding to an intensity of ∼50 GW cm^{-2}.)

Spectra taken from $ncFAPbBr_3@SiO_2$ films at different pump wavelengths between 1300–1740 nm, a selection of which are plotted in Fig. 3a (shaded areas), show sharp peaks at the third harmonic wavelength in the range 450–570 nm. These peaks have an intensity that depends on the frequency of the pump field, as shown in Fig. 3b. As a reference, the third harmonic spectra of a 1 mm thick glass microscope slide are also measured to factor out the fluctuations in intensity and beam-diameter of the laser pump beam. Glass is characterized by a spectrally flat nonlinear susceptibility,[24] with value $\chi^{(3)glass}$ = $(1.6 \pm 0.2) \times 10^{-22}$ m V^{-2} (measured *via* THG).[25]

The absolute efficiency of the generated third harmonic from a $ncFAPbBr_3@SiO_2$ composite film is reported in Fig. 3b. The absolute efficiency, η, is measured from $\eta = P_3^{composite}/P_1^{laser}$, where $P_3^{composite}$ is the measured power of the third harmonic signal of the sample. A maximum conversion efficiency of 4.27×10^{-6} is attained for excitation at 1560 nm. In addition, the nature of the THG signal transmitted through the film is verified by recording the polarization of the generated third harmonic from the $ncFAPbBr_3@SiO_2$ films as shown in Fig. 3c, which, as expected, preserves the linear polarisation of the incident beam. Furthermore, by measuring the intensity of the generated third harmonic signal as a function of the excitation power, the characteristic cubic-dependence of a third-order effect is confirmed, as shown in Fig. 3d.

Extraction of nonlinear susceptibility

From the experimental spectral measurements of the THG signal from the $ncFAPbBr_3@SiO_2$ film in the wavelength range 1340–1740 nm, the spectral behaviour of the third-order
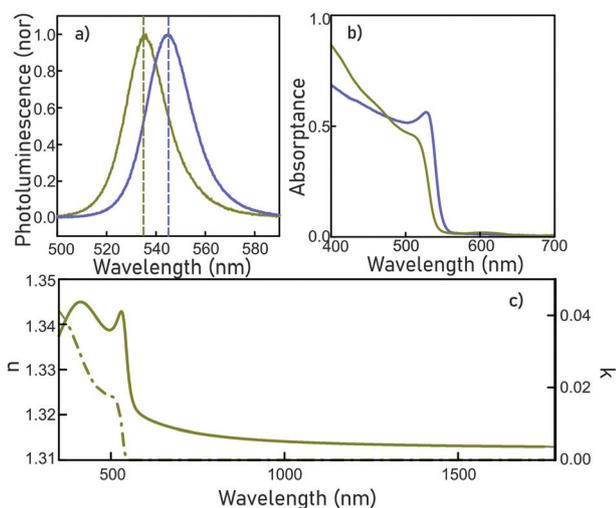

Fig. 2 Linear optics measurements. (a) Normalised photoluminescence spectra of $ncFAPbBr_3@SiO_2$ and a $FAPbBr_3$ bulk films (green and blue lines, respectively). Dotted lines indicate the spectral position of the PL maxima and are just a guide for the eye. (b) Absorptance of $ncFAPbBr_3@SiO_2$ and $FAPbBr_3$ bulk films (green and blue lines, respectively). (c) Refractive index and extinction coefficient (solid and dotted lines respectively) of a $ncFAPbBr_3@SiO_2$ film.
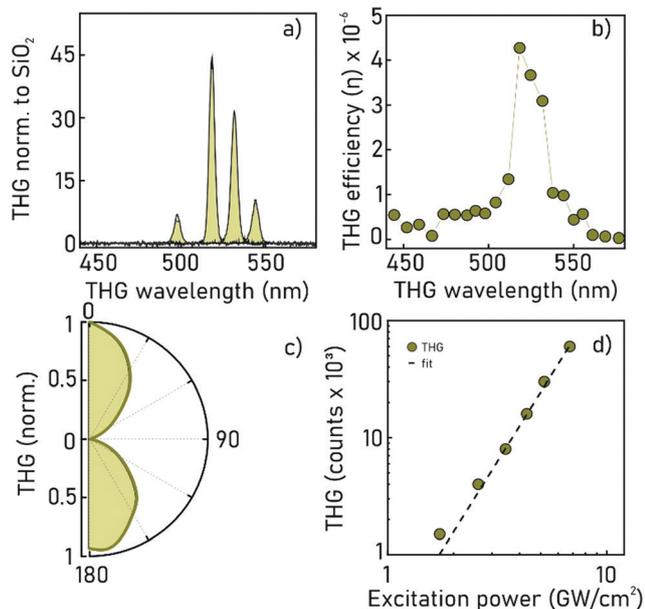
15992 | *J. Mater. Chem. C*, 2020, **8**, 15990–15995

This journal is © The Royal Society of Chemistry 2020

Fig. 3 THG from ncFAPbBr$_3$@SiO$_2$ film. (a) Spectra of selected third harmonic emission lines attained from the film. Results are normalised to the THG maximum efficiency of silica glass. (b) Absolute THG efficiency from a ncFAPbBr$_3$@SiO$_2$ film. (c) Polarisation analysis of the third harmonic beam (λ_1 = 1540 nm, λ_3 = 513 nm). (d) Log–log plot of the third harmonic beam intensity *versus* pump power at λ_1 = 1500 nm for the ncFAPbBr$_3$@-SiO$_2$ film. The fitting (dashed line) demonstrates a linear dependence with slope 3 on the excitation power.

susceptibility of the FAPbBr$_3$ nanocrystals, $\chi^{(3)\text{NC}}$, can be extracted. In order to do so, we employ an analytical solution of nonlinear Maxwell's equations used to model the intensity of the third harmonic emission, I_3, from thin films.[26] The model is applicable when the pump is neither depleted in the film because of the nonlinear process (a common assumption when the energy conversion has low efficiency), nor is attenuated by linear absorption. The model also assumes plane waves, which is a very good approximation in our case where the pump is not tightly focused, and the thickness of the sample is of the order of the wavelength. The model also uses the slowly-varying amplitude approximation.

$$I_3 = f(\lambda, L)|\chi^{(3)}|^2 I_1^3, \tag{1}$$

In expression (1), $\chi^{(3)}$ is the third-order nonlinear susceptibility of the film, I_1 is the pump intensity and the thickness (L) dependent function, $f(\lambda, L)$, is given by:

$$f(\lambda, L) = A\left(\frac{e^{-2\alpha_3 L} - 2\cos(\Delta k L)e^{-\alpha_3 L} + 1}{\alpha_3^2 + \Delta k^2}\right)e^{-2\alpha_3 L}, \tag{2}$$

where $A = (9\omega^2)/(16|\tilde{n}_3|n_1^3 \varepsilon_0^2 c^4)$ is a constant encompassing the real part of the refractive index of the material at the pump frequency, n_1, and its complex refractive index at the third harmonic wavelength, $\tilde{n}_3$. The physical constants c and ε_0 are the vacuum speed of light and permittivity, respectively. In eqn (2), α_3 is the absorption coefficient of the third harmonic wave and Δk is the phase mismatch between the pump and third harmonic wave. These quantities are dependent on the linear optical properties of the composite nanocrystal film

(shown in Fig. 2c). The absorption coefficient of the third-harmonic wave is given by:

$$\alpha_3 = \frac{2\pi\kappa_3}{\lambda_3}, \tag{3}$$

which is dependent upon the extinction coefficient, κ_3, at the third harmonic wavelength, λ_3. The phase mismatch is given by:

$$\Delta k = \frac{6\pi(n_1 - n_3)}{\lambda_1}, \tag{4}$$

where n_1 and n_3 are the real part of the refractive index at the pump wavelength (λ_1) and third harmonic wavelength (λ_3) respectively.

Based on our determination of the dielectric constant of the composite film, we can now plot the spectral behaviour of $\alpha(\lambda)$ and $\Delta k(\lambda)$ in the selected experimental range. This is done in Fig. 4a, where $\alpha(\lambda)$ is drawn as a green solid line and, as expected, falls off abruptly for energies below the electronic bandgap. The phase mismatch $\Delta k(\lambda)$ (grey dashed line) follows the same spectral behaviour of the real part of the linear refractive index of the ncFAPbBr$_3$@SiO$_2$ film (Fig. 2c), presenting a sharp increase for energies above the bandgap.
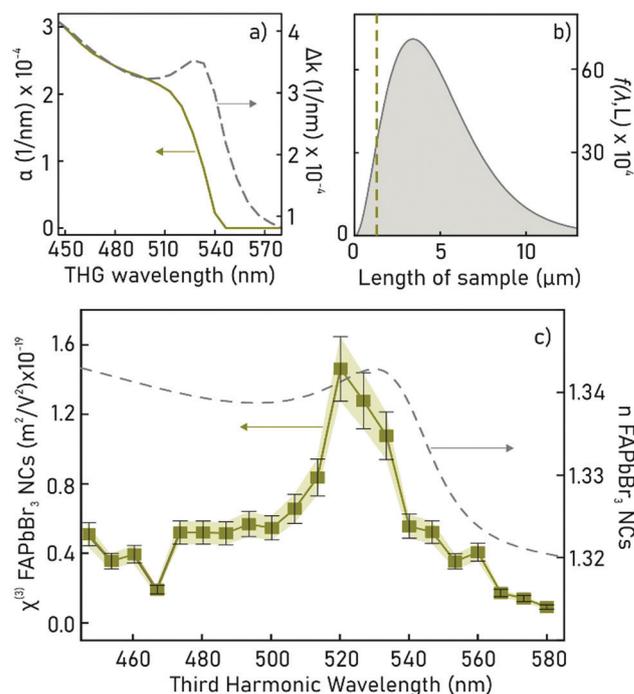

Fig. 4 Extraction of third-order nonlinear susceptibility ($\chi^{(3)\text{NC}}$) of a ncFAPbBr$_3$@SiO$_2$ film. (a) Spectral behaviour of the absorption coefficient of the third harmonic wave and the phase mismatch between the fundamental and the third harmonic waves. (b) Calculated $f(\lambda, L)$, which is proportional to third harmonic intensity, *versus* ncFAPbBr$_3$@SiO$_2$ film thickness (λ_1 = 1560 nm, λ_3 = 520 nm). The vertical dashed line indicates the actual thickness of the composite film (1300 nm). (c) Spectral dependence of both the estimated third order nonlinear susceptibility of the FAPbBr$_3$ nanocrystals after volume correction and the linear refractive index of the composite (dashed line).

This journal is © The Royal Society of Chemistry 2020

J. Mater. Chem. C, 2020, **8**, 15990–15995 | **15993**

We then study the effects of film thickness L on the modelled function, $f(\lambda,L)$, given by eqn (2) and that determines the effect of the excitation length on the generated third harmonic, as indicated by eqn (1). For a fixed pump wavelength of 1560 nm, where the maximum THG intensity from the ncFAPbBr$_3$@SiO$_2$ composite film is experimentally observed, the length dependency of $f(\lambda,L)$ is shown in Fig. 4b. THG has a quick raise and a sharp decrease for L larger than the absorption length in the medium, as show in Fig. 4b. The green dashed line indicates the thickness of the composite FAPbBr$_3$ nanocrystal film (which is 1300 nm). Our model reveals that the efficiency of the THG from the composite FAPbBr$_3$ nanocrystal film could be further increased by a factor of around 2 by fine tuning the film thickness.

Finally, the extraction of the third-order susceptibility of the composite film ($\chi^{(3)\text{composite}}$), at each measured pump wavelength in the range 1340–1740 nm, can be extracted from the experimental values of the peak THG intensity from the ncFAPbBr$_3$@SiO$_2$ film with eqn (1). In order to account for the spectral fluctuations of the pump intensity, I_1, in this equation, we take a ratio of the generated THG by the composite nanocrystal film to the THG generated by the microscope slide. This ensures that I_1 is kept the same across the spectral measurements for both the sample and the reference, hence the fluctuations across different wavelengths can be cancelled out when taking the ratio (see ESI†). From this, an absolute value of $\chi^{(3)\text{composite}}$ is found by multiplying by the spectrally-flat third-order nonlinear susceptibility of glass, $\chi^{(3)\text{glass}}$. Knowing that the volume filling fraction of perovskite nanocrystals in the composite film is $ff_{\text{NC}} = 0.065$, we can estimate the spectrally dependent third-order nonlinear susceptibility of ncFAPbBr$_3$, $\chi^{(3)\text{NC}}$, shown in Fig. 4c. This treatment assumes that the $\chi^{(3)\text{NC}}$ is much greater than that of the encapsulating SiO$_2$ matrix. In this approximation the third-order susceptibility of ncFAPbBr$_3$ is:

$$\left|\chi^{(3)\text{NC}}(\lambda)\right| = \frac{\left|\chi^{(3)\text{composite}}\right|}{ff_{\text{NC}}} \tag{5}$$

In Fig. 4c, we show the spectral behaviour of $\chi^{(3)\text{NC}}$. A clear peak in $\chi^{(3)\text{NC}}$ at $1.46 \pm 0.19 \times 10^{-19}$ m^2 V^{-2} is evident for frequencies around $\lambda_3 = 520$ nm ($\lambda_1 = 1560$ nm), which is also close to the frequency of the excitonic resonance of the nanocrystals, as it can be seen when compared to the composite $n(\lambda)$ curve (green line), which is also plotted in Fig. 4c. Please note that at this wavelength, the absorption length ($1/\alpha$) is shorter than the coherence length ($2\pi/\Delta k$) (see Fig. 4a), and therefore the third harmonic oscillations within the composite film are exponentially attenuated.

Conclusions

We have found experimental evidence of nonlinear third harmonic generation from organic lead halide perovskite nanocrystals. Full characterization of the dependence of the efficiency of this process was performed for FAPbBr$_3$ nanocrystals embedded in a porous film for a wide range of near infrared excitation wavelengths, as well as an analysis of the effect of

film thickness. A detailed characterization of the optical constants of the composite allows us to establish that maximum nonlinear conversion is achieved at the excitonic resonance, for which a third-order nonlinear susceptibility of $1.46 \pm 0.19 \times 10^{-19}$ m^2 V^{-2} (1.04×10^{-11} esu) is reported, which is, to the best of our knowledge, the largest reported for organic cation based perovskite nanocrystals so far, and of the same order than the best ones reported for purely inorganic colloidal perovskite nanocrystals. Our work expands the range of optoelectronic applications of perovskite quantum dots, already widely studied in the fields of solar energy conversion and lighting, to that of nonlinear optics.

Conflicts of interest

There are no conflicts to declare.

Acknowledgements

Notes and references

1 J. Xu, X. Li, J. Xiong, C. Yuan, S. Semin, T. Rasing and X.-H. Bu, *Adv. Mater.*, 2019, 1806736.

2 B. Wenger, P. K. Nayak, X. Wen, S. V. Kesava, N. K. Noel and H. J. Snaith, *Nat. Commun.*, 2017, **8**, 590.

3 E. J. Juarez-Perez, R. S. Sanchez, L. Badia, G. Garcia-Belmonte, Y. Soo Kang, I. Mora-Sero and J. Bisquert, *J. Phys. Chem. Lett.*, 2014, **5**, 2390.

4 X. Chen, H. Lu, Y. Yang and M. C. Beard, *J. Phys. Chem. Lett.*, 2018, **9**, 2595.

5 O. A. Lozhkina, V. I. Yudin, A. A. Murashkina, V. V. Shilovskikh, V. G. Davydov, R. Kevorkyants, A. V. Emeline, Y. V. Kapitonov and D. W. Bahnemann, *J. Phys. Chem. Lett.*, 2018, **9**, 302.

6 D. Marongiu, M. Saba, F. Quochi, A. Mura and G. Bongiovanni, *J. Mater. Chem. C*, 2019, **7**, 12006.

7 X. Chen, Y. Wang, J. Song, X. Li, J. Xu, H. Zeng and H. Sun, *J. Mater. Chem. C*, 2019, **123**, 10564.

8 D. J. Clark, C. C. Stoumpos, F. O. Saouma, M. G. Kanatzidis and J. I. Jang, *Phys. Rev. B*, 2016, **93**, 195202.

9 J. C. Johnson, Z. Li, P. F. Ndione and K. Zhu, *J. Mater. Chem. C*, 2016, **4**, 4847.

10 I. Abdelwahab, G. Grinblat, K. Leng, Y. Li, X. Chi, A. Rusydi, S. A. Maier and K. Ping Loh, *ACS Nano*, 2018, **12**, 644.

11 C. Yi, J. Luo, S. Meloni, A. Boziki, N. Ashari-Astani, C. Grätzel, S. M. Zakeeruddin, U. Röthlisberger and M. Grätzel, *Energy Environ. Sci.*, 2016, **9**, 656.

12 B. Park, B. Philippe, S. M. Jain, X. Zhang, T. Edvinsson, H. Rensmo, B. Zietz and G. Boschloo, *J. Mater. Chem. A*, 2015, **3**, 21760.

15994 | *J. Mater. Chem. C*, 2020, **8**, 15990–15995

This journal is © The Royal Society of Chemistry 2020

13 D. Myung Jang, K. Park, D. Hwan Kim, J. Park, F. Shojaei, H. Seok Kang, J.-P. Ahn, J. Woon Lee and J. Kyu Song, *Nano Lett.*, 2015, **15**, 5191.

14 J. Li, L. Xu, T. Wang, J. Song, J. Chen, J. Xue, Y. Dong, B. Cai, Q. Shan, B. Han and H. Zeng, *Adv. Mater.*, 2017, **29**, 1603885.

15 J. Yang, Z. Liu, M. Pi, H. Lin, F. Zeng, Y. Bian, T. Shi, J. Du, Y. Leng and X. Tang, *Adv. Opt. Mater.*, 2020, **8**, 2000290.

16 Y. Wang, X. Li, X. Zhao, L. Xiao, H. Zeng and H. Sun, *Nano Lett.*, 2016, **16**, 448.

17 S. Liu, G. Chen, Y. Huang, S. Lin, Y. Zhang, M. He, W. Xiang and X. Liang, *J. Alloys Compd.*, 2017, **724**, 889.

18 A. Rubino, M. Anaya, J. F. Galisteo-López, T. C. Rojas, C. M. E. Calvo and H. Míguez, *ACS Appl. Mater. Interfaces*, 2018, **10**, 38334.

19 S. ten Brinck, F. Zaccaria and I. Infante, *ACS Energy Lett.*, 2019, **4**, 2739.

20 M. Anaya, A. Rubino, T. C. Rojas, J. F. Galisteo-López, M. E. Calvo and H. Míguez, *Adv. Opt. Mater.*, 2017, **5**, 1601087.

21 A. Rubino, L. Caliò, A. García-Bennett, M. E. Calvo and H. Míguez, *Adv. Opt. Mater.*, 2020, **8**, 1901868.

22 J. Ávila, C. Momblona, P. Boix, M. Sessolo, M. Anaya, G. Lozano, K. Vandewal, H. Míguez and H. J. Bolink, *Energy Environ. Sci.*, 2018, **11**, 3292.

23 A. R. Forouhi and I. Bloomer, *Phys. Rev. B: Condens. Matter Mater. Phys.*, 1986, **34**, 7018.

24 D. Milam, *Appl. Opt.*, 1998, **37**, 546.

25 U. Gubler and C. Bosshard, *Phys. Rev. B: Condens. Matter Mater. Phys.*, 2000, **61**, 10702.

26 N. Youngblood, R. Peng, A. Nemilentsau, T. Low and M. Li, *ACS Photonics*, 2017, **4**, 8.

This journal is © The Royal Society of Chemistry 2020

J. Mater. Chem. C, 2020, **8**, 15990–15995 | **15995**